Available online at www.sciencedirect.com
ScienceDirect
Journal of Solid State Chemistry 181 (2008) 1017–1024
JOURNAL OF SOLID STATE CHEMISTRY
www.elsevier.com/locate/jssc

Synthesis, crystal structure and properties of two 1D nano-chain coordination polymers constructed by lanthanide with pyridine-3,4-dicarboxylic acid and 1,10-phenanthroline

Hui-Hua Song[a,*], Ya-Juan Li[a], You Song[b], Zhan-Gang Han[a], Fang Yang[a]

[a]*College of Chemistry and Material Sciences, Hebei Normal University, Shijiazhuang 050016, PR China*
[b]*State Key Laboratory of Coordination Chemistry, Coordination Chemistry Institute, Nanjing University, Nanjing 210093, PR China*

Received 31 July 2007; received in revised form 14 December 2007; accepted 30 December 2007
Available online 12 January 2008

Abstract

The hydrothermal reactions of $LnCl_3 \cdot 6H_2O$ (Ln = Eu, Tb), pyridine-3,4-dicarboxylic acid (3,4-pydaH$_2$), 1,10-phenthroline (phen) and NaOH in aqueous medium yield two metal-organic hybrid materials, $[Eu_2(3,4\text{-pyda})_3(phen)(H_2O) \cdot H_2O]_n$ (**1**) and $[Tb_2(3,4\text{-pyda})_3(phen)(H_2O) \cdot H_2O]_n$ (**2**), respectively. Both compounds have similar topology structure containing one-dimensional nano-chain, which is further assembled into a three-dimensional supramolecular network via π–π stacking interactions and hydrogen bonds. To the best of our knowledge, they represent the first example of nano-chain coordination polymers constructed by 3,4-pydaH$_2$ and chelate heterocylic ligand. Interestingly, the 3,4-pyda anion exhibits three kinds of coordination modes in these complexes. The coordination modes of 3,4-pyda in complexes **1** and **2** have not been observed in other coordination polymers containing 3,4-pyda ligands. Compounds **1** and **2** exhibit strong fluorescent emission bands in the solid state at room temperature. Their magnetic analyses show that they exhibit different magnetic interactions.

Keywords: Lanthanide (III); Crystal structure; Luminescent property; Magnetic property; Hydrothermal synthesis; Carboxylate

1. Introduction

The rational design and construction of novel coordination polymer have attracted much attention in the field of supramolecular chemistry and crystal engineering, due to their intriguing topologies and potential applications as functional materials [1–6]. Multicarboxylate ligands have been widely used for exhibiting various coordination modes to finish various structures with honeycomb, brick-wall, rectangular grid, bilayer, ladder, diamonds and open frameworks [7–10]. As a member of multicarboxylate ligands containing N-donor, pyridine-3,4-dicarboxylic acid has unique features compared to *p*-pyridinecarboxylic acid and *m*-pyridinecarboxylic acid, showing an excellent building block with charge and multi-connecting ability [11,12]. Moreover, previous studies are mainly focused on those of transition and post-transition elements including Mn, Cu and Zn [11–16], but those with lanthanide complexes are less reported. However, owing to the large radii, high coordination numbers and special magnetic and fluorescence properties of the lanthanides, lanthanide complexes are likely to bring unprecedented crystal structures and unique properties [17–20]. Therefore, it is interesting to study new lanthanide complexes with pyridine-3,4-dicarboxylate. Herein, we report the two new lanthanide coordination polymers $[M_2(3,4\text{-pyda})_3(phen)(H_2O) \cdot H_2O]_n$ (M = Eu (**1**) and Tb (**2**), 3,4-pydaH$_2$ = pyridine-3,4-dicarboxylic acid, phen = 1,10-phenthroline), in which two double-chains are linked by water molecules and pyda ligands into interesting one-dimensional nano-chain structures. To the best of our knowledge, they represent the first example of nano-chain coordination polymers constructed by 3,4-pydaH$_2$ and chelate heterocylic ligand.

*Corresponding author.
E-mail address: songhuihua@mail.hebtu.edu.cn (H.-H. Song).

0022-4596/$ - see front matter © 2008 Elsevier Inc. All rights reserved.
doi:10.1016/j.jssc.2007.12.039

Furthermore, both show intense luminescent properties at room temperature. Their magnetic analyses show that they exhibit different magnetic interactions.

2. Experimental section

2.1. Materials and measurements

$LnCl_3 \cdot 6H_2O$ (Ln = Eu, Tb) were prepared by dissolving their respective oxides in concentrated hydrochloric acid followed by drying. All the other reagents were commercially available and were used as received without further purification. Elemental analyses were performed with an Elemental Vario EL elemental analyzer. IR spectra were (KBr pellets) recorded in the 4000–400 cm^{-1} range with an FTIR-8900 spectrometer. Thermogravimetric analysis (TGA) was performed on a TGA-7 instrument in flowing N_2 with a heating rate of 15 °C min^{-1}. Fluorescent spectra were measured with a Hitachi F-4500 luminescence spectrometer. Magnetic measurements were carried out with a SQUID MPMS-XL7 magnetometer.

2.2. Synthesis of $[Eu_2(3,4\text{-pyda})_3(phen)(H_2O)\cdot H_2O]_n$ (1)

A mixture of $EuCl_3 \cdot 6H_2O$ (0.2 mmol), pyridine-3,4-dicarboxylic acid (0.3 mmol), phen (0.3 mmol) and NaOH (0.6 mmol) and H_2O (8.0 mL) was sealed in a 15-mL Teflon reactor, which was heated to 170 °C for 3 days and then slowly cooled to room temperature by air cooling. Colorless needle-like single crystals of compound **1** suitable for X-ray single-crystal diffraction analysis were obtained (yield 57%). *Anal. calc.* for $C_{33}H_{21}Eu_2N_5O_{14}$: C 39.03, H 2.08, N 6.95; found: C 39.15, H 1.95, N 6.90. IR (KBr, cm^{-1}): 3464m (ν_{OH}), 1646s ($\nu_{c=N(phen)}$), 1602s (ν^{as}_{coo}), 1566s (ν^{as}_{coo}), 1491m (ν^{as}_{coo}), 1426s (ν^{s}_{coo}), 1394s (ν^{s}_{coo}), 845m ($\nu_{C-H(phen)}$), 730m ($\nu_{C-H(phen)}$).

2.3. Synthesis of $[Tb_2(3,4\text{-pyda})_3(phen)(H_2O)\cdot H_2O]_n$ (2)

Compound **2** was prepared using a similar method to that employed for the synthesis of compound **1**, with $TbCl_3 \cdot 6H_2O$ (0.2 mmol) in place of $EuCl_3 \cdot 6H_2O$. Colorless needle-like single crystals of compound **2** suitable for X-ray single-crystal diffraction analysis were obtained (yield 62%). *Anal. calc.* for $C_{33}H_{21}Tb_2N_5O_{14}$: C 38.14, H 1.81, N 6.74; found: C 38.50, H 2.06, N 6.80. IR (KBr, cm^{-1}): 3474m (ν_{OH}), 1646s ($\nu_{c=N(phen)}$), 1602s (ν^{as}_{coo}), 1566s (ν^{as}_{coo}), 1491m (ν^{as}_{coo}), 1426s (ν^{s}_{coo}), 1394s (ν^{s}_{coo}), 845m ($\nu_{C-H(phen)}$), 730m ($\nu_{C-H(phen)}$).

2.4. X-ray crystallography

Data for compound **1** were measured on a Rigaku Saturn CCD diffractometer with Mo$K\alpha$ radiation (λ = 0.71073 Å) at 293(2) K, while data for compound **2** were measured on a Bruker SMART-CCD area detector diffractometer with Mo$K\alpha$ radiation (λ = 0.71073 Å) at 294(2) K. Both structures were solved by direct methods. All non-hydrogen atoms were refined anisotropically by full-matrix least-squares methods. The hydrogen atoms were added geometrically and were not refined. All calculations were performed using SHELXS-97 and SHELXL-97 [21,22]. A summary of the crystallographic data and refinement parameters is given in Table 1. The selected bond lengths and angles for **1** and **2** are given in Tables 2 and 3, respectively.

Table 1
Crystal data and structure refinement details

Compound	**1**	**2**
Empirical formula	$C_{33}H_{21}Eu_2N_5O_{14}$	$C_{33}H_{21}Tb_2N_5O_{14}$
Formula weight	1015.47	1029.39
Temperature (K)	293(2)	294(2)
Wavelength (Å)	0.71073	0.71073
Crystal system	Triclinic	Triclinic
Space group	$P\bar{1}$	$P\bar{1}$
a (Å)	*7.5670(15)*	7.5288(10)
b (Å)	12.662(3)	12.6329(18)
c (Å)	18.384(4)	18.320(3)
α (deg)	70.82(3)	70.680(2)
β (deg)	78.96(3)	79.074(2)
γ (deg)	76.02(3)	76.231(2)
V (Å^3)	1602.2(6)	1585.3(4)
Z	2	2
Calculated density (Mg/m^3)	2.105	2.156
$F(000)$	984	992
Absorption coefficient (mm^{-1})	3.963	4.510
θ Range for data collection (deg)	1.74–27.86	1.19 26.39
Limiting indices	$-9\leqslant h\leqslant 9$, $-16\leqslant k\leqslant 14$ $-24\leqslant l\leqslant 18$	$-4\leqslant h\leqslant 9$, $-15\leqslant k\leqslant 15$ $-22\leqslant l\leqslant 22$
Reflections collected/ unique (R_{int})	12411/7514	9161/6393 (0.0337)
Completeness to $\theta = 27.86°$	98.5%	(θ = 26.39°)98.3%
Max. and min. transmission	0.7969 and 0.6478	1.000000 and 0.603171
Data/restraints/ parameters	7514/3/487	6393/3/487
Goodness-of-fit on F^2	1.030	1.004
Final R indices [$I>2\sigma(I)$]	$R1 = 0.0321$ w$R2 = 0.0779$	$R1 = 0.0347$ w$R2 = 0.0775$
R indices (all data)	$R1 = 0.0436$ w$R2 = 0.0808$	$R1 = 0.0561$ w$R2 = 0.0861$
Largest diff. peak and hole (e Å^{-3})	0.692 and −2.132	1.629 and −1.395

3. Results and discussion

3.1. Crystal structures of 1 and 2

Compound **1** shows a one-dimensional chain structure in which the asymmetric unit contains two europium atoms, three 3,4-pyda ligands, one phen ligand, one coordination water molecule and one lattice water molecule.

Table 2
Selected bond lengths (Å) and angles (deg) for compound **1**

Eu(1)–O(4)#1	2.305(3)	Eu(2)–O(12)#1	2.336(4)	Eu(1)–O(5)	2.370(3)
Eu(1)–O(11)#1	2.370(3)	Eu(2)–O(9)	2.429(4)	Eu(2)–O(6)#3	2.409(4)
Eu(1)–O(3)#2	2.399(3)	Eu(1)–O(7)	2.370(3)	Eu(2)–O(10)	2.454(3)
Eu(1)–O(13)#2	2.582(3)	Eu(2)–O(1)	2.491(3)	Eu(1)–O(2)	2.520(3)
Eu(2)–O(8)	2.566(4)	Eu(2)–O(7)	2.583(3)	Eu(1)–O(1)	2.632(3)
Eu(2)–N(4)	2.609(4)	Eu(1)–O(13)	2.645(3)	Eu(2)–N(5)	2.614(4)
O(3)–Eu(1)#2	2.399(3)	Eu(1)–Eu(2)	4.1417(16)	O(6)–Eu(2)#1	2.409(4)
O(4)–Eu(1)#3	2.305(3)	Eu(1)–Eu(1)#2	4.4249(14)	O(11)–Eu(1)#3	2.370(3)
O(12)–Eu(2)#3	2.337(3)	O(13)–Eu(1)#2	2.582(3)		
O(11)#1–Eu(1)–O(7)	81.46(12)	O(4)#1–Eu(1)–O(3)#2	86.02(12)		
O(5)–Eu(1)–O(3)#2	78.51(12)	O(11)#1–Eu(1)–O(3)#2	148.39(11)		
O(7)–Eu(1)–O(3)#2	92.15(12)	O(4)#1–Eu(1)–O(2)	81.60(11)		
O(5)–Eu(1)–O(2)	135.89(12)	O(11)#1–Eu(1)–O(2)	70.11(12)		
O(7)–Eu(1)–O(2)	116.62(11)	O(3)#2–Eu(1)–O(2)	138.15(12)		
O(4)#1–Eu(1)–O(13)#2	74.57(11)	O(5)–Eu(1)–O(13)#2	140.16(11)		
O(11)#1–Eu(1)–O(13)#2	133.99(12)	O(7)–Eu(1)–O(13)#2	131.45(11)		
O(3)#2–Eu(1)–O(13)#2	71.90(11)	O(2)–Eu(1)–O(13)#2	66.29(11)		
O(4)#1–Eu(1)–O(1)	131.32(11)	O(5)–Eu(1)–O(1)	129.39(11)		
O(11)#1–Eu(1)–O(1)	72.32(11)	O(7)–Eu(1)–O(1)	67.50(11)		
O(3)#2–Eu(1)–O(1)	133.42(11)	O(2)–Eu(1)–O(1)	50.40(11)		
O(13)#2–Eu(1)–O(1)	90.45(10)	O(4)#1–Eu(1)–O(13)	136.73(11)		
O(5)–Eu(1)–O(13)	127.96(12)	O(11)#1–Eu(1)–O(13)	133.26(10)		
O(7)–Eu(1)–O(13)	67.13(11)	O(3)#2–Eu(1)–O(13)	69.35(10)		
O(2)–Eu(1)–O(13)	93.42(11)	O(13)#2–Eu(1)–O(13)	64.33(12)		
O(1)–Eu(1)–O(13)	64.18(10)	O(6)#3–Eu(2)–O(9)	118.65(11)		
O(12)#1–Eu(2)–O(6)#3	147.03(11)	O(12)#1–Eu(2)–O(9)	73.21(12)		
O(12)#1–Eu(2)—O(10)	125.73(12)	O(6)#3–Eu(2)–O(10)	78.07(11)		
O(9)–Eu(2)–O(10)	53.90(11)	O(12)#1–Eu(2)–O(1)	80.93(12)		
O(6)#3–Eu(2)–O(1)	74.72(12)	O(9)–Eu(2)–O(1)	72.68(11)		
O(10)–Eu(2)–O(1)	93.14(11)	O(12)#1–Eu(2)–O(8)	75.78(13)		
O(6)#3–Eu(2)–O(8)	95.27(12)	O(9)–Eu(2)–O(8)	145.81(13)		
O(10)–Eu(2)–O(8)	147.37(12)	O(1)–Eu(2)–O(8)	116.14(11)		
O(12)#1–Eu(2)–O(7)	75.44(11)	O(6)#3–Eu(2)–O(7)	74.67(10)		
O(9)–Eu(2)–O(7)	131.56(11)	O(10)–Eu(2)–O(7)	149.45(11)		
O(1)–Eu(2)–O(7)	66.63(11)	O(8)–Eu(2)–O(7)	50.24(10)		
O(12)#1–Eu(2)–N(4)	78.03(13)	O(6)#3–Eu(2)–N(4)	133.98(13)		
O(9)–Eu(2)–N(4)	72.51(13)	O(10)–Eu(2)–N(4)	75.65(12)		
O(1)–Eu(2)–N(4)	143.21(13)	O(8)–Eu(2)–N(4)	87.37(12)		
O(7)–Eu(2)–N(4)	134.18(11)	O(12)#1–Eu(2)–N(5)	125.35(13)		
O(6)#3–Eu(2)–N(5)	76.44(13)	O(9)–Eu(2)–N(5)	122.67(12)		
O(10)–Eu(2)–N(5)	80.87(12)	O(1)–Eu(2)–N(5)	151.15(13)		
O(8)–Eu(2)–N(5)	66.55(12)	O(7)–Eu(2)–N(5)	105.52(12)		
N(4)–Eu(2)–N(5)	62.63(14)				

Symmetry codes. #1: $x+1$, y, z ; #2: $-x+1$, $-y+1$, $-z$; #3: $x-1$, y, z.

As illustrated in Fig. 1, the two crystallographically unique Eu centers exhibit different coordination environments in **1**. Eu1 is coordinated by seven O atoms [Eu1–O(3,4-pyda) = 2.370(3)–2.632(3) Å] coming from five different 3,4-pyda units and two O atoms [Eu1–O(H_2O) = 2.582(3)–2.645(3) Å] coming from two coordinated water molecules, showing a distorted triply capped trigonal prism geometry with O–Eu1–O bond angles ranging from 50.4(11) to 148.39(12)°. Whereas Eu2 center is ligated by seven O atoms [Eu2–O(pyda) = 2.336(4)–2.583(3) Å] coming from five different 3,4-pyda unit and two N atoms [Eu2–O(phen) = 2.609(4)–2.614(4) Å] coming from two phen ligands to complete a distorted triply capped trigonal prism configuration with O–Eu2–O bond angles ranging from 50.24(10)° to 149.45(11)°. The Eu1 and Eu2 atoms are bridged by three 3,4-pyda ligands to form the building block [Eu_2(3,4-pyda)$_3$(phen)(H_2O)]. The two building blocks connect head to head via coordination water [O13 and O13A] and two pyda ligands to form tetranuclear Eu_4(3,4-pyda)$_6$(phen)$_2$(H_2O)$_2$ subunits, which are interconnected through the 3,4-pyda ligands to form an infinite belt-like chain along the *a*-axis as shown in Fig. 2. The distances of the Eu⋯Eu separation are 4.142 Å for Eu1⋯Eu2 and 4.425 Å for Eu1⋯Eu1. The Eu ions in one chain distributed in a broad zone with width of 9.748 Å. The phen molecules located at both sides of the chain as wings. The separation of neighboring phen on the same side is ca. 7.567 Å and the dihedral angle between the phen planes is 0°. The plane of phen is not perpendicular with that composed of ions, ca. 78.96°. The phen enlarged the dimensions of the chain into

Table 3
Selected bond lengths (Å) and angles (deg) for compound **2**

Tb(1)–O(2)#1	2.292(4)	Tb(1)–O(9)	2.342(4)	Tb(1)–O(5)	2.348(4)
O(2)–Tb(1)#1	2.292(4)	O(4)–Tb(1)#2	2.614(4)	Tb(2)–O(10)#3	2.317(4)
Tb(1)–O(4)#2	2.506(4)	Tb(1)–O(7)	2.350(4)	Tb(1)–O(3)#2	2.614(4)
Tb(1)–O(13)#2	2.560(4)	Tb(2)–O(12)	2.405(5)	Tb(2)–O(11)	2.431(4)
Tb(2)–O(8)	2.387(4)	Tb(2)–N(4)	2.575(5)	Tb(1)–O(1)	2.376(4)
Tb(2)–N(5)	2.591(5)	Tb(1)–O(13)	2.560(4)	Tb(2)–O(5)#3	2.564(4)
Tb(2)–O(4)#1	2.470(4)	O(13)–Tb(1)#2	4.1417(16)	Tb(2)–O(6)#3	2.558(5)
O(4)–Tb(2)#1	2.470(4)	O(3)–Tb(1)#2	2.506(4)	O(6)–Tb(2)#4	2.558(5)
O(10)–Tb(2)#4	2.317(4)	O(5)–Tb(2)#4	2.564(4)		
O(2)#1–Tb(1)–O(9)	85.73(15)	O(2)#1–Tb(1)–O(5)	152.11(14)		
O(9)–Tb(1)–O(5)	81.68(14)	O(2)#1–Tb(1)–O(7)	77.25(14)		
O(9)–Tb(1)–O(7)	69.95(15)	O(5)–Tb(1)–O(7)	75.07(14)		
O(9)–Tb(1)–O(1)	148.09(15)	O(2)#1–Tb(1)–O(1)	85.49(15)		
O(5)–Tb(1)–O(1)	92.19(14)	O(7)–Tb(1)–O(1)	78.21(14)		
O(2)#1–Tb(1)–O(3)#2	81.56(15)	O(9)–Tb(1)–O(3)#2	70.26(15)		
O(9)–Tb(1)–O(13)#2	134.08(14)	O(5)–Tb(1)–O(13)#2	131.05(13)		
O(7)–Tb(1)–O(13)#2	140.03(14)	O(1)–Tb(1)–O(13)#2	72.00(14)		
O(3)#2–Tb(1)–O(13)#2	66.16(14)	O(2)#1–Tb(1)–O(4)#2	131.47(14)		
O(9)–Tb(1)–O(4)#2	72.14(14)	O(5)–Tb(1)–O(4)#2	67.31(13)		
O(7)–Tb(1)–O(4)#2	129.38(13)	O(1)–Tb(1)–O(4)#2	133.90(13)		
O(13)#2–Tb(1)–O(4)#2	90.58(12)	O(2)#1–Tb(1)–O(13)	136.25(13)		
O(9)–Tb(1)–O(13)	133.26(13)	O(5)–Tb(1)–O(13)	67.13(13)		
O(7)–Tb(1)–O(13)	128.48(14)	O(1)–Tb(1)–O(13)	69.86(13)		
O(3)#2–Tb(1)–O(4)#2	50.61(13)	O(3)#2–Tb(1)–O(13)	93.09(14)		
O(13)#2–Tb(1)–O(13)	63.92(14)	O(10)#3–Tb(2)–O(8)	147.09(15)		
O(12)–Tb(2)–O(11)	54.23(14)	O(10)#3–Tb(2)–O(4)#1	81.04(14)		
O(8)–Tb(2)–O(4)#1	74.71(14)	O(12)–Tb(2)–O(4)#1	72.46(14)		
O(11)–Tb(2)–O(4)#1	93.39(14)	O(10)#3–Tb(2)–O(6)#3	75.62(16)		
O(8)–Tb(2)–O(6)#3	95.47(15)	O(12)–Tb(2)–O(6)#3	145.70(15)		
O(11)–Tb(2)–O(6)#3	146.97(14)	O(4)#1–Tb(2)–O(6)#3	116.35(14)		
O(10)#3–Tb(2)–O(5)#3	75.51(14)	O(8)–Tb(2)–O(5)#3	74.57(14)		
O(12)–Tb(2)–O(5)#3	131.27(13)	O(11)–Tb(2)–O(5)#3	149.35(13)		
O(4)#1–Tb(2)–O(5)#3	66.45(13)	O(6)#3–Tb(2)–O(5)#3	50.66(13)		
O(10)#3–Tb(2)–N(4)	124.95(16)	O(8)–Tb(2)–N(4)	76.61(15)		
O(12)–Tb(2)–N(4)	123.05(16)	O(11)–Tb(2)–N(4)	80.89(16)		
O(4)#1–Tb(2)–N(4)	151.32(15)	O(6)#3–Tb(2)–N(4)	66.13(16)		
O(5)#3–Tb(2)–N(4)	105.43(15)	O(10)#3–Tb(2)–N(5)	77.67(16)		
O(8)–Tb(2)–N(5)	134.27(15)	O(12)–Tb(2)–N(5)	72.54(16)		
O(11)–Tb(2)–N(5)	75.64(15)	O(4)#1–Tb(2)–N(5)	142.96(16)		
O(6)#3–Tb(2)–N(5)	87.16(15)	O(5)#3–Tb(2)–N(5)	134.30(15)		
N(4)–Tb(2)–N(5)	62.86(17)				

Symmetry codes. #1: $-x, -y+1, -z+2$; #2: $-x+1, -y+1, -z+2$; #3: $x-1, y, z$.; #4: $x+1, y, z$.

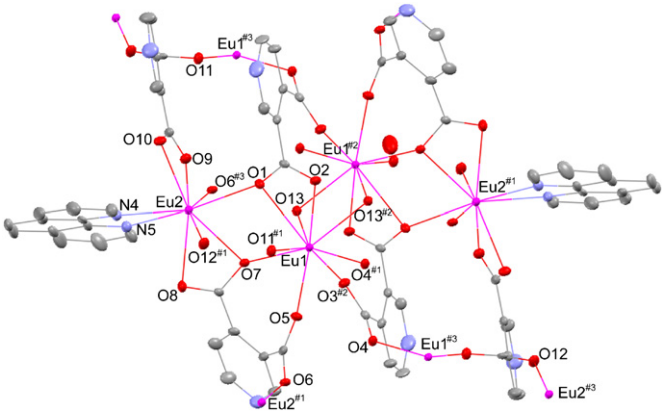

Fig. 1. The ORTEP drawing for compound **1** with the atom-labeling scheme. Symmetry codes: #1 $x+1, y, z$; #2 $-x+1, -y+1, -z$; 3 $x-1, y, z$.

ca. 21.393 Å. So the polymeric structure of **1** can also be described as those two double-chains are connected by water molecules and 3,4-pyda ligands into interesting one-dimensional nano-chain structures.

It should be noteworthy that carboxylate groups of 3,4-pyda ligands adopt three kinds of coordination modes: (1) the 3,4-pyda anion acts as cheating-bridging tetradentate ligand towards the three Eu(III) cation (Scheme 1(a)), with four carboxylic oxygen; (2) the 3,4-pyda anion acts as cheating–cheating–bridging tetradentate ligand towards the three Eu(III) cation (Scheme 1(b)), with four carboxylic oxygen; (3) the 3,4-pyda anion acts as bridging–cheating–bridging tetradentate ligand towards the four Eu(III) cation (Scheme 1(c)), with four carboxylic oxygen. Interestingly, in three cases pyridine nitrogen atom

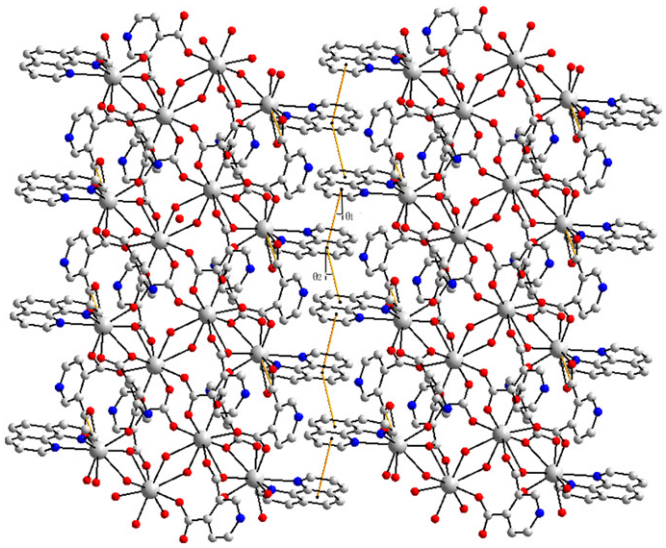

Fig. 2. The two-dimensional layered structures of compound **1**, $\theta_1 = 5.4°$; $\theta_2 = 19.3°$.

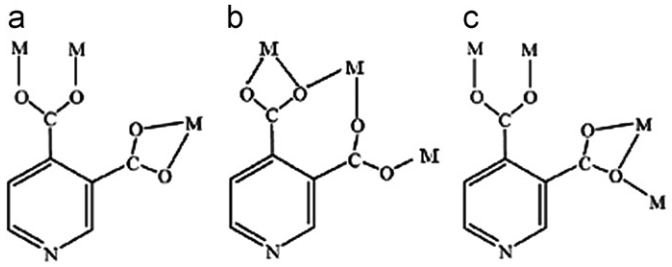

Scheme 1. The coordination modes of pyda ligand in compounds **1** and **2**.

does not participate in coordination. To the best of our knowledge, the coordination modes of 3,4-pyda in complex **1** have not been observed in other coordination polymers containing 3,4-pyda ligands [2,5,8–15]. The three types of 3,4-pyda ligands play a key role in extending the chains.

There are π–π stacking interactions of the aromatic ring of phen ligands from two adjacent nano-chain structures with face-to-face distances of ca. 3.624–3.661 Å, leading to the formation of extended 2D layer parallel to the *ab* plane as shown in Fig. 2. These layers are further extended into three-dimensional supramolecular architecture through hydrogen bonding interactions between the free water molecules and the O atom of the 3,4-pyda carboxylate or N atom of the 3,4-pyda (Fig. 3). The typical hydrogen bonds are O13⋯O14($-x+1$, $-y+1$, $-z$) 2.874 Å, O14⋯N2($x-1$, $y+1$, z) 2.936 Å and O13⋯O6($x-1$, y, z) 2.852 Å (Table 4).

X-ray single-crystal diffraction studies reveal that compound **2** adopts a structure very similar to that of **1** (Figs. S1, S2, S3), as shown by the detailed structural data listed in the Supplementary Materials.

3.2. Thermal stability

To investigate their thermal stabilities, TGA of **1** and **2** were carried out at a heating rate of 10 °C min^{-1} (Figs. S4, S5). TG analysis shows that the thermal decomposition behavior of compounds **1** and **2** was similar. Compound **1** first lost weight corresponding to two water molecules (observed 3.52%, calculated 3.55%) from 150 to 250 °C. Further weight loss corresponding to all organic components (observed 62.78%, calculated 61.80%) was observed between 250 and 900 °C. The remaining weight of 33.70% corresponds to the percentage (34.65%) of Eu and O components, indicating that the final product is Eu_2O_3.

Compound **2** first lost weight corresponding to two water molecules (observed 3.54%, calculated 3.50%) from 150 to 250 °C, Further weight loss corresponding to all organic components (observed 59.75%, calculated 60.18%) was observed between 250 and 930 °C, The remaining weight of 36.71% corresponds to the percentage (36.32%) of Tb and O components, indicating that the final product is Tb_4O_7.

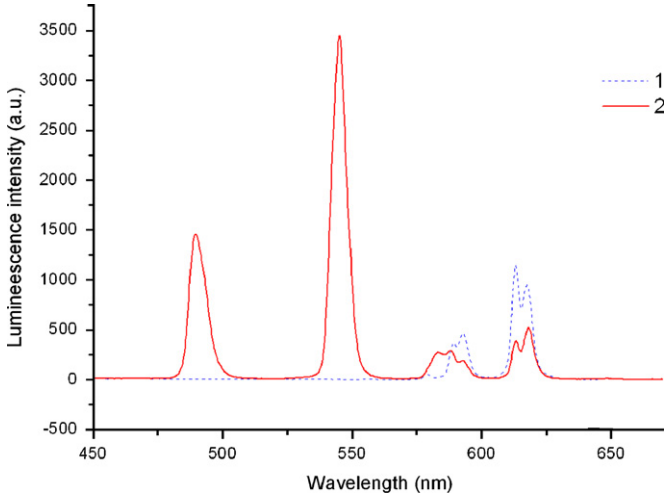

Fig. 3. The emission spectra (emission at 340 nm) of compounds **1** and **2** in the solid state.

Table 4
Hydrogen bonding distances (Å) and angle (deg) data for **1** and **2**

D–H	d(H⋯A)	<DHA	d(D⋯A)	Symmetry transformation for A
1				
O13–H13A⋯O14	1.913	170.73	2.874	$-x+1$, $-y+1$, $-z$
O13–H13B⋯O6	1.980	148.34	2.852	$x-1$, y, z
O14–H14A⋯N2	2.498	112.89	2.936	$x-1$, $y+1$, z
2				
O13–H13A⋯O14	2.138	152.72	2.919	x, y, $z+1$
O13–H13A⋯O3	2.287	115.96	2.766	x, y, $z+1$
O13–H13B⋯O8	2.061	150.90	2.834	$x+1$, y, z

3.3. Photoluminescent properties

The emission spectra of compounds **1** and **2** in solid state at room temperature are depicted in Fig. 4. Excitation at 340 nm into the lowest energy ligand-centered absorption band results in the luminescence characteristic of the Ln^{3+}

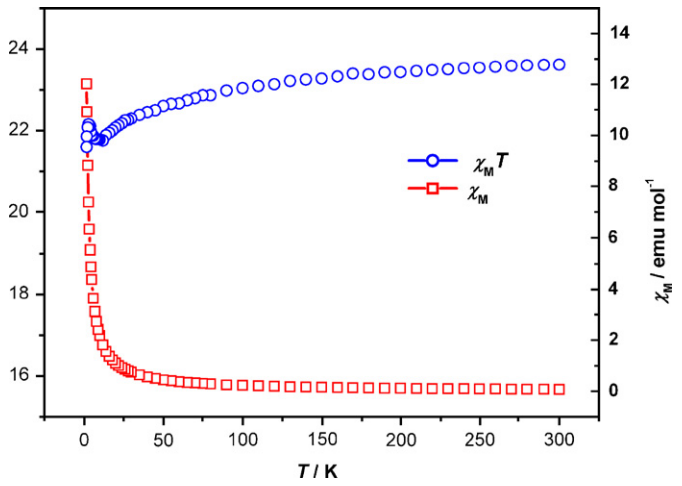

Fig. 4. Temperature dependence of magnetic properties of **2**. Solid lines are the guide for eyes.

ion (Ln = Eu, Tb). The emission peaks of **1** at 578, 589, 593, 613 and 617 nm can be assigned to $^5D_0 \rightarrow {}^7F_j$ ($j = 0, 1, 2$) transitions of Eu^{3+} [23–27]. The symmetric forbidden emission $^5D_0 \rightarrow {}^7F_0$ found at 578 nm indicate that more than one coordination environments are present for Eu(III). The dominant band in the emission spectrum is the $^5D_0 \rightarrow {}^7F_2$ electronic dipole transition, which was split into two levels at 613 and 617 nm. The $^5D_0 \rightarrow {}^7F_2$ transition is hypersensitive transition and is extremely sensitive to chemical bonds in the vicinity of Eu^{3+} ion. The intensity of the $^5D_0 \rightarrow {}^7F_2$ transition increases as the site symmetry of Eu^{3+} decreases [28]. The $^5D_0 \rightarrow {}^7F_1$ emission peak was also split into two levels at 589 and 593 nm. The $^5D_0 \rightarrow {}^7F_1$ transition is a magnetic dipole transition which is fairly insensitive to the coordination environment of the Eu^{3+} ion. It is interesting to note that the $^5D_0 \rightarrow {}^7F_2$ transition is much more intense than the $^5D_0 \rightarrow {}^7F_1$ transition and the intensity ratio $I(^5D_0 \rightarrow {}^7F_2)/I(^5D_0 \rightarrow {}^7F_1)$ is equal to ca. 2.0, which indicating that the symmetry of the Eu^{3+} ion site is low. Because the asymmetric microenvironment causes the polarization of the Eu(III) ion under the influence of the electric field of the surrounding ligands and thus increases the probability for the electronic dipole transition [27].

Compound **2** gives an entirely typical Tb^{3+} emission spectrum containing the expected sequence of $^5D_4 \rightarrow {}^7F_j$ transitions, with the $j = 3$–6 components being visible. Specific assignments [23–26] are as follows: $^5D_4 \rightarrow {}^7F_6$ (490 nm), $^5D_4 \rightarrow {}^7F_5$(545 nm), $^5D_4 \rightarrow {}^7F_4$(594 nm) and $^5D_4 \rightarrow {}^7F_3$(618 nm). Among the peaks, the emissions at 594 nm from $^5D_4 \rightarrow {}^7F_4$ and at 618 nm from the $^5D_4 \rightarrow {}^7F_3$ show signs of splitting, which may be the result of the different coordination environment of the Tb(III) ion [29]. In addition, the spectrum is dominated by the $^5D_4 \rightarrow {}^7F_5$ transition, which gives an intense green luminescence output for the solid sample. These are in agreement with the result of the single-crystal X-ray analysis.

Generally, it is possible to obtain detectable luminescence for Eu(III) and Tb(III) only by direct excitation at their absorption peaks (at 396 and 370 nm, respectively) [26,30,31]. The fact is that, for both **1** and **2**, strong luminescence was observed by excitation at 340 nm indicating that we have succeeded in increasing the absorption cross section of both lanthanides by excitation of the ligand(s) and energy transfer to the Ln^{3+} ion by an indirect process (antenna effect).

3.4. Magnetic properties

Variable-temperature magnetic susceptibility measurements were performed on a SQUID MPMS-XL7 at an applied field of 1 kG using crystalline samples of **1** and **2** in the range of 300 to 1.8 K in the forms of $\chi_M T$ and χ_M versus T as shown in Figs. 5 and 6. At room temperature, $\chi_M T$ of compound **2** is 23.61 emu K mol^{-1}, consistent with the value of 23.625 emu K mol^{-1} expected for two non-interacting Tb^{III} ions including the significant contribution of the 4f orbital ($4f^8$, $J = 6$, $S = 3$, $L = 3$, $g = 3/2$, $^7F_6$). As the system is cooled, $\chi_M T$ slowly decreases and reaches a

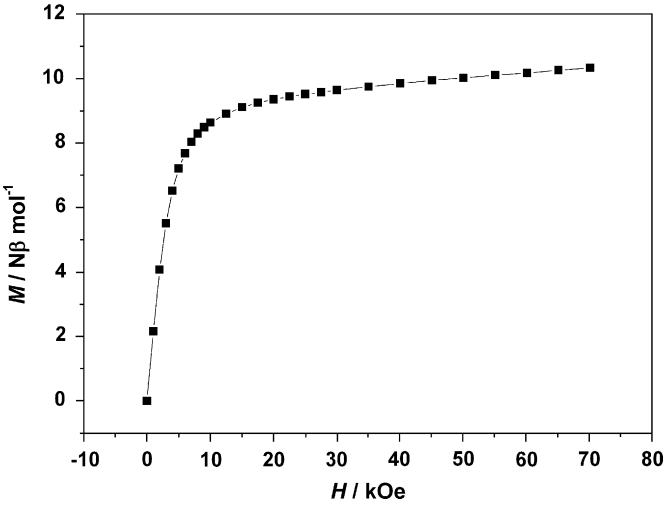

Fig. 5. Field dependence of magnetization of **2**. Solid lines are the guide for eyes.

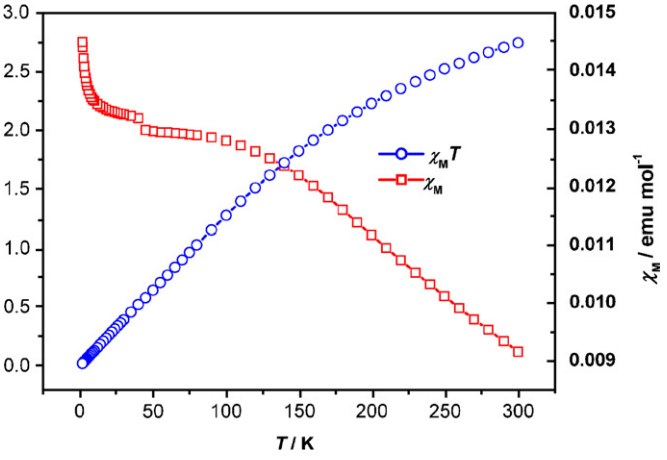

Fig. 6. Temperature dependence of magnetic properties of **1**. Solid lines are the guide for eyes.

minimum value of 21.76 emu K mol^{-1} at 12 K, which is obviously ascribed to the thermal depopulation of the Stark components of lanthanide ions at low temperatures [28,32–34]. Below 12 K, $\chi_M T$ quickly increases to a maximum of 22.15 emu K mol^{-1} at 3 K and then abruptly decreases, indicating the ferromagnetic coupling between Tb^{III} ions. The maximum of $\chi_M T$ is even lower than the value at room temperature, indicating that the ferromagnetic coupling is very weak but it is strong enough to compensate for effect due to the thermal depopulation of the Stark levels [34]. Fig. 6 shows the M–H plot at 1.8 K. Under the applied field, the magnetization first quickly and then slowly increases below and above 10 kOe but it is far away from the saturation state of 18 Nβ mol^{-1} ($M = \Sigma gJ = 2 \times 3/2 \times 6$) at 70 kOe, suggesting the strong anisotropy in **2** because of the belt-like structure.

For compound **1**, $\chi_M T$ at room temperature is 2.75 emu K mol^{-1} corresponding to the population of an excited state (the theoretical value is 3 emu K mol^{-1}) based on two Eu^{III} ions. As the temperature cool down, $\chi_M T$ monotonously decreases, which is also attributed to the thermal depopulation of the Stark components of free Eu ions the same as that in compound **2**. However, for **1**, the Stark effect dominates the magnetic properties rather than the spin–spin coupling because the lowest lying J multiplet of the free Eu ion is close to the excited ones (only 350 cm^{-1} from the ground state to first excited state) [33]. At 1.8 K $\chi_M T$ is equal to 0.02 emu K mol^{-1} close to zero, indicating a ground state of $^7F_0$ of Eu^{III} ions, because of $\chi_M T \propto J(J+1)$ (Fig. 6).

4. Conclusion

In this paper, two novel lanthanide coordination polymers $\{[M_2(3,4\text{-pyda})_3(\text{phen})H_2O] \cdot H_2O\}_n (M = \text{Eu, Tb})$ have been synthesized under hydrothermal condition. X-ray diffraction reveals that both compounds have similar topology structures containing one-dimensional nano-chain that are further assembled into a three-dimensional supramolecular network via π–π stacking interactions and hydrogen bonds. The three coordination modes of 3,4-pyda in the two compounds are different from those found in other coordination polymers containing 3,4-pyda ligands. To our knowledge, they represent the first example of nano-chain coordination polymers constructed by 3,4-pydcH_2 and chelate heterocylic ligand. Compounds **1** and **2** show characteristic transitions of Eu^{3+} and Tb^{3+}, respectively, and they show different magnetic properties.

Supplementary data

Crystallographic data for the structure reported in this paper have been deposited with Cambridge Crystallographic Data Center as supplementary publication No. CCDC-648470 for compound **1** and CCDC-648466 for compound **2**. Copies of the data can be obtained free of charge on applying to CCDC, 12 Union Road, Cambridge CB2 1EZ, UK (fax: +44 1223 336 033; e-mail: deposit@ccdc.cam.ac.uk)

Acknowledgments

This work was supported by the Natural Science Foundation of China (Grant no. 20601007), the Natural Science Foundation of Hebei Education Department (Grant no. ZH2006002).

Appendix A. Supplementary materials

Supplementary data associated with this article can be found in the online version at doi:10.1016/j.jssc.2007.12.039.

References

[1] S.T. Wilson, B.M. Lok, C.A. Messian, T.R. Cannan, E.M. Flanigen, J. Am. Chem. Soc. 104 (1982) 1146.
[2] K. Inoue, H. Imai, P.S. Ghalsasi, K. Kikuchi, M. Ohba, H. Okawa, J.V. Yakhmi, Angew. Chem. Int. Ed. 40 (2001) 4242.
[3] P.J. Hagrman, D. Hagrman, J. Zubieta, Angew. Chem. Int. Ed. 38 (1999) 2639.
[4] S. Noro, S. Kitagawa, M. Kondo, K. Seki, Angew. Chem. Int. Ed. 39 (2000) 2081.
[5] D. Cave, J.M. Gascon, A.D. Bond, S.J. Teat, P.T. Wood, Chem. Commun. (2002) 1050.
[6] X.L. Wang, C. Qin, E.B. Wang, Y.G. Li, N. H, C.W. Hu, L. Xu, Inorg. Chem. 43 (2004) 1850.
[7] L. Pan, B.S. Finkel, X.-Y. Huang, J. Li, Chem. Commun. (2001) 105.
[8] L.R. Macgillivray, R.H. Groeneman, J.L. Atwood, J. Am. Chem. Soc. 120 (1998) 2676.
[9] O.M. Yaghi, H. Li, J. Am. Chem. Soc. 117 (1995) 10401.
[10] P.J. Hagrman, D. Hagrman, J. Zubieta, Angew. Chem. Int. Ed. 38 (1999) 2638.
[11] W. Chen, Q. Xue, C. Chen, H.-M. Yuan, W. Xu, J.-S. Chen, S.-N. Wang, J. Dalton Trans. (2003) 28.
[12] Q.Z. Zhang, C.Z. Lu, C.K. Xia, Inorg. Chem. Commun. 8 (2005) 304.
[13] M.L. Tong, J. Wang, S. Hu, J. Solid State Chem. 178 (2005) 1518.
[14] Y.F. Zhou, C.Y. Yue, D.Q. Yuan, L. Chen, J.T. Chen, A.J. Lan, F.L. Jiang, M.C. Hong, Eur. J. Inorg. Chem. (2006) 4852.
[15] X.L. Wang, C. Qin, E.B. Wang, Y.G. Li, N. H, C.W. Hu, L. Xu, Chem. Comm. (2004) 378.
[16] X.L. Wang, C. Qin, E.B. Wang, Y.G. Li, N. H, C.W. Hu, L. Xu, Inorg. Chem. 43 (2004) 1850.
[17] Y.Z. Zheng, M.L. Tong, X.M. Chen, Eur. J. Inorg. Chem. (2005) 4109.
[18] X.L. Wang, C. Qin, E.B. Wang, L. Xu, Inorg. Chim. Acta 359 (2006) 417.
[19] Z.B. Han, X.N. Cheng, X.F. Li, X.M. Chen, Z. Anorg. Allg. Chem. 631 (2005) 937.
[20] D. Ang, G.B. Deacon, P.C. Junk, D.R. Turner, Polyhedron 26 (2007) 385.
[21] G.M. Sheldrick, Acta Crystallogr. A 46 (1990) 467.
[22] G.M. Sheldrick, SHELXS-97, a program for X-ray crystal structure solution, and SHELXL-97, A Program for X-ray Structure Refinement, Gottingen University, Germany, 1997.
[23] Few representative references: S.W. Magennis, S. Parsons, Z. Pikramenou, Chem. Eur. J. 8 (2002) 5761.
[24] V. Patroniak, P.N.W. Baxter, J.-M. Lehn, Z. Hnatejko, M. Kubicki, Eur. J. Inorg. Chem. (2004) 2379.

[25] C. Tedeschi, J. Aze'ma, H. Gornitzka, P. Tisnes, C. Picard, Dalton Trans. (2003) 1738.
[26] K.A. Thiakou, V. Bekiari, C.P. Raptopoulou, V. Psycharis, P. Lianos, S.P. Perlepes, Polyhedron 25 (2006) 2869.
[27] Z.Q. Bian, K.Z. Wang, L.P. Jin, Polyhedron 21 (2002) 313.
[28] J.-C.G. Bunzli, G.R. Choppin, Lanthanide Probers in Life, Chemical and Earth Science, Elsevier, Amsterdam, 1989 (Chapter 7).
[29] Z. Wang, C.M. Jin, T. Shao, Inorg. Chem. Commun. 5 (2002) 642.
[30] M. Dejneka, E. Snitzer, R.E. Riman, J. Lumin. 65 (1995) 227.
[31] B.C. Joshi, J. Non-Cryst. Solids 180 (1995) 217.
[32] J.-P. Costes, F. Nicodème, Chem. Eur. J. 8 (2002) 3442.
[33] C. Benelli, D. Gatteschi, Chem. Rev. 102 (2002) 2369.
[34] Z.H. Zhang, Y. Song, T.A. Okamura, Y. Hasegawa, W.Y. Sun, N. Ueyama, Inorg. Chem. 45 (2006) 2896.